Journal of Materials Chemistry C

SnO/β-Ga2O3 heterojunction barrier Schottky diodes for depressed reverse leakage current and improved breakdown voltage

Journal:	*Journal of Materials Chemistry C*
Manuscript ID	TC-COM-03-2025-001355.R1
Article Type:	Communication
Date Submitted by the Author:	16-Apr-2025
Complete List of Authors:	Wang, Jun; Hefei University of Technology Yao, Xin-Wang; Hefei University of Technology Xu, Xiu-Xing; Hefei University of Technology Wu, Xia; Hefei University of Technology Qian, Jun-Han; Hefei University of Technology Liu, Yan-Fang; Hefei University of Technology Wu, Chunyan; Hefei University of Technology Luo, Linbao; Hefei University of Technology, Department of Applied Physics Wang, Xiujuan; Hefei University of Technology, School of Microelectronics

SCHOLARONE™
Manuscripts

SnO/β-Ga_2O_3 heterojunction barrier Schottky diodes for depressed reverse leakage current and improved breakdown voltage

Jun Wang,[a] Xin-Wang Yao,[a] Xiu-Xing Xu,[a] Xia Wu,[a] Jun-Han Qian,[a] Xiu-Juan Wang,[a] Yan-Fang Liu, *[b] Lin-Bao Luo[a] and Chun-Yan Wu*[a]

[a] *School of Microelectronics, Hefei University of Technology, Hefei 230009, China*

[b] *Instrumental Analysis center, Hefei University of Technology, Hefei 230009, China*

* Corresponding author. Email: dragon_lyf@hfut.edu.cn; cywu@hfut.edu.cn (C. Y. Wu).

ABSTRACT

In this article, we report a vertical β-Ga_2O_3 heterojunction barrier Schottky (HJBS) diode fabricated by selective growth of circular p-type SnO film array through the reactive magnetron sputtering. Compared to its Schottky barrier diode (SBD) counterpart, the HJBS diode shows a slightly increased turn-on voltage (V_{on}) and the specific on-resistance ($R_{on,sp}$), but its breakdown voltage (BV) is greatly improved due to the depressed electric field crowding effect at the anode edge as well as the lateral surface depletion effect of the SnO/β-Ga_2O_3 p-n junction. A high BV of 1375 V and a Baliga's power figure of merit (PFOM) of 0.37 GW/cm^2 are achieved for the device with the spacing of 3 μm, which are expected to be improved by further shrinking the spacing. Meanwhile, the reverse leakage current (J_R) is lower than 2 μA/cm^2 (the detection limit of the system) even at a reverse bias (V_R) of 1250 V. The SnO/β-Ga_2O_3 HJBS diodes show great potential in the future β-Ga_2O_3 power electronic devices with high PFOM while maintaining a suppressed reverse leakage current.

Keywords: β-Ga_2O_3, heterojunction barrier Schottky diode (HJBS), power electronic device

β-Ga_2O_3 is a promising semiconductor for high-power electronics due to its ultrawide bandgap (4.6-4.9 eV), high critical breakdown electric field (8 MV/cm), and large Baliga's figure of merit (BFOM, >3000) with respect to Si.[1,2] The availability of high-quality single crystals from low-cost melt-grown technology also benefits the future mass production of β-Ga_2O_3 based power devices.[3] Schottky barrier diodes (SBD) and p-n heterojunction diode (HJD) are two basic types of β-Ga_2O_3 based power devices.[4,5] The unipolar SBD is featured as lower turn-on voltages (V_{on}) and faster recovery times, which facilitates their application in high-voltage and high-speed switching devices. However, the lower barrier height also results in a higher reverse leakage current (J_R) at a high reverse voltage (V_R) and a limited breakdown voltage (BV). For the HJD, the depletion of p-n junction at a high V_R greatly suppressed the J_R and improved the BV, but the accompanying large V_{on} leads to a relatively large conduction loss. This goes against the requirements of practical high-efficiency application. To combine the low conduction loss of SBD and the distinguished voltage blocking ability of HJD, the heterojunction barrier Schottky diode (HJBS) is proposed by introducing periodic p-n heterojunction regions underneath the Schottky anode. The Schottky junction will conduct before the p-n heterojunctions at low forward voltage, leading to a V_{on} closed to SBD, while the depletion of the p-n heterojunction regions will shield the Schottky contact from the high V_R, thereby suppressing the J_R.[6,7] For example, Lv et al.[8] demonstrated the first vertical β-Ga_2O_3 HJBS diode with thermally oxidized p-type NiO, which has a similar or slightly higher V_{on} and $R_{on,sp}$ compared to the SBD as well as a dramatically increased BV. To fully function the p-islands, Yan et al.[9] embedded

p-NiO_x between the periodic β-Ga_2O_3 fin structures. Despite of the etching damage, the HJBS diode presented a low $R_{on,sp}$ of 1.94 mΩ·cm² with a high BV of 1.34 kV at a β-Ga_2O_3 fin width of 3 μm.

Notably, although a variety of oxides, including Cu_2O,[10] Ir_2O_3[11] and SnO,[12] have been reported for the fabrication of all-oxide β-Ga_2O_3 HJD other than NiO/β-Ga_2O_3, research on the HJBS diodes is still to be developed. Herein, SnO, a p-type oxide with a direct bandgap of ~2.9 eV and hole mobility about one order of magnitude higher than NiO,[13,14] is adopted for the fabrication of β-Ga_2O_3 HJBS diode. The HJBS diode with the spacing of 3 μm shows V_{on} of 1.2 V and $R_{on,sp}$ of 5.1 mΩ·cm², which are slightly inferior to the control SBD, but the BV is remarkably improved to 1375 V, giving a Baliga's power figure of merit (PFOM) of 0.37 GW/cm^2. The voltage blocking is expected to be further improved with the shrinking spacing, revealing the potential application of the SnO/β-Ga_2O_3 heterojunction in the future β-Ga_2O_3 power electronic devices.

Figure 1(a) presents the cross-sectional schematic of the β-Ga_2O_3 HJBS diode. A piece of commercially available (001)-oriented β-Ga_2O_3 epitaxial wafer from Novel Crystal Technology, Inc. (5 mm×5mm), consisted of a 10-μm-thick epitaxial layer with Sn doping concentration of about 2×10^{16} cm^{-3} on a heavily doped substrate, was used for the fabrication of the HJBS diode. The rear surface of the precleaned substrate was treated in Ar plasma for 30 s to enhance the n-type doping and Ti/Au (20/80 nm) stack was then deposited by electron beam evaporation, followed by a rapid thermal annealing in N_2 ambient at 540°C for 1 min to form the Ohmic contact. Circular p-type

SnO array was patterned through photolithography and deposited *via* reactive magnetron sputtering from a high-purity Sn target in the mixture of Ar/O_2 with oxygen partial pressure P_O of 2%. The sputtering power was set as 50 W and the chamber pressure was maintained at 0.4 Pa. 10-min annealing at 200°C was adopted to obtain a better crystallinity.[15] Finally, Ni/Au (30/100 nm) stack with a diameter of 170 μm was deposited through photolithography and electron beam evaporation to act as the anode electrode. An SBD without SnO layer and a SnO/β-Ga_2O_3 heterojunction diode (HJD) were also fabricated for comparison (shown in Figure S1).

Top-view optical microphotograph of a typical device is shown in Figure 1(b). The width (W) of the SnO stripes and the spacing between the stripes (L) are measured to be approximately 2.93 μm and 3.16 μm, respectively, and the thickness of the SnO is approximately 105 nm (Figure 1(c)). The outermost one shows the width of 20 μm, functioning as the junction termination extension (JTE). Figure 1(d) shows XRD pattern of the SnO film, which can be well indexed as tetragonal SnO (JCPDS card No. 06-0395).[16] X-ray photoelectron spectroscopy (XPS) is further employed to verify the composition of the film. The Sn 3d core-level XPS spectrum (shown in Figure 1(e)) exhibits two peaks located at 494.3 eV and 485.9 eV, respectively, which are well consistent with the previously reported binding energies of Sn^{2+}. The peak of O 1s core level spectrum at 529.8 eV (shown in Figure 1(f)) can also be assigned to O-Sn^{2+}, suggesting the high-purity of the obtained SnO film.[17] Further, Hall hole concentrations (p_h) and Hall mobilities (μ_h) of the obtained SnO film are determined to be 5×10^{17} cm^{-3} and 7 cm^2/(V·s) *via* van-der-Pauw Hall measurement. This is consistent

with the reported value in the literature.[18] Notably, the hole mobility is about one orders of magnitude higher than that of magnetron sputtered NiO film with similar hole concentrations (for example, 0.94 cm^2/(V·s)[19] and 0.87 cm^2/(V·s)[20]).

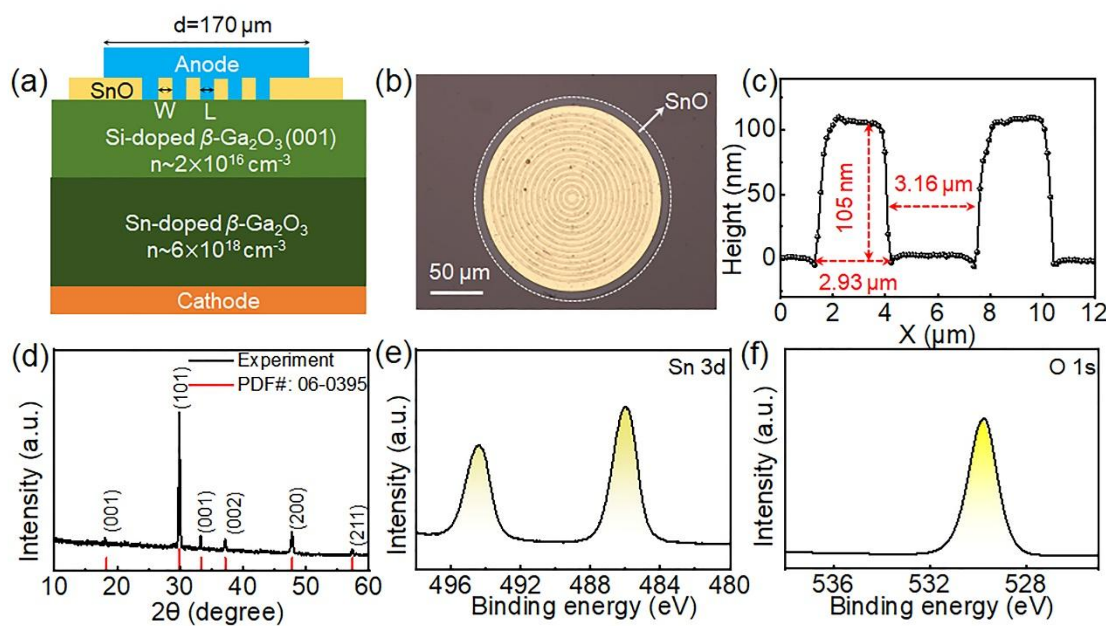

Fig. 1. (a) Cross-sectional schematic and (b) top-view optical microphotograph of a typical vertical β-Ga_2O_3 JBS diode. (c) Height profile of circular p-SnO film extracted from (b). (d) XRD pattern of SnO film. (e) Sn 3d and (f) O 1s core-level XPS spectra of SnO film.

Figure 2(a) presents UV-vis absorption spectrum of the SnO film, which shows dramatic absorption in the UV region. The $(\alpha h\nu)^2$ *versus* $h\nu$ curve (inset in Figure 2(a)) gives a direct optical bandgap of 2.9 eV, which is in accordance with the reported value in the literature.[21-23] Figure 2(b) depicts the UPS spectrum of the SnO film. To ensure accurate measurement, the Fermi level of the instrument was calibrated using Au reference sample prior to the test. The secondary electron cutoff is positioned at about 5.1 eV by linear extrapolation of the edge, showing the work function of 5.1 eV for SnO film. Furthermore, the valence band maximum (VBM) of the SnO film is

determined to be about 1.0 eV, which means that the VBM is located 1.0 eV below the Fermi level and reveals the p-type conductivity of the SnO film. VBM of β-Ga_2O_3 is determined to be about 4.4 eV (Figure 2(c)). Considering the electron affinity ($\chi = 4$ eV) and band gap ($E_g = 4.8$ eV),[24] the work function (W) of β-Ga_2O_3 is then determined to be about 4.4 eV and a type-II heterojunction is expected to be formed between SnO film and β-Ga_2O_3 (Figure 2(d)), showing the conduction band offset ($\triangle E_C$) of 0.8 eV. The theoretical built-in potential (qV_{bi}) is calculated to be about 0.7 eV based on the difference in the Fermi level (E_F) of SnO and β-Ga_2O_3. Therefore, the electrons in β-Ga_2O_3 side need to overcome the potential barrier (V_a=V_{bi}+$\triangle E_C/q$) of 1.5 eV to inject into the SnO side. This is much smaller than that of NiO/β-Ga_2O_3 heterojunction (3.6 eV) and suggests a potential lower turn-on voltage.[25]

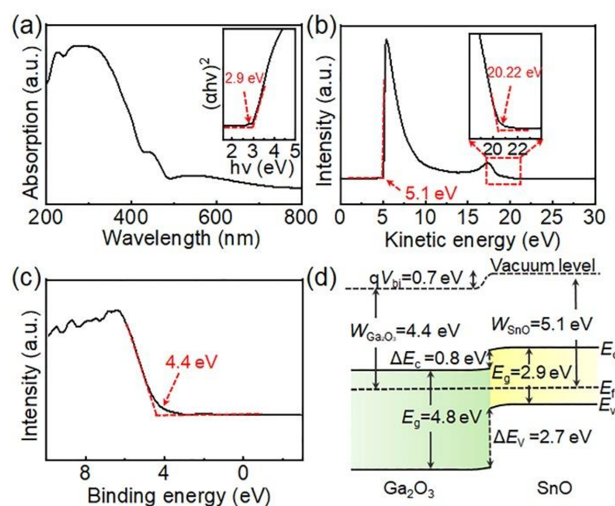

Fig.2. (a) Absorption spectrum of the SnO film. Inset shows the plot of $(ahv)^2$ *versus* *hv*. (b) UPS spectra of the SnO film. (c) VBM spectrum of the β-Ga_2O_3 substrate. (d) Schematic energy band diagram of the SnO/β-Ga_2O_3 heterojunction.

The forward and reverse current-voltage (J-V) characteristics of the devices are measured using Keysight B1500A and B1505A Semiconductor Device Analyzer,

respectively. Figure 3(a) present the forward *J-V* curves and the $R_{on,sp}$ of β-Ga_2O_3 HJBS diodes as well as its SBD and HJD counterparts. All diodes exhibit a high ON-OFF current ratio (I_{on}/I_{off}) of around 10^{11}(shown in Figure S2), showing an excellent rectifying characteristic. The forward current (J_F) at a 5 V forward voltage (V_F) of the HJBS diode reaches 600 A/cm^2 and the minimal $R_{on,sp}$ is 5.1 mΩ·cm^2, slightly inferior to those of the SBD (932 A/cm^2 and 3.6 mΩ·cm^2) but superior to those of the HJD (336 A/cm^2 and 8.1 mΩ·cm^2). Further, the V_{on} of the HJBS diode is linear extrapolated to be 1.2 V, which is 0.2 V higher than that of the SBD and 0.3 V lower than that of the HJD. The *J-V* characteristics are quantitatively analyzed following the thermionic emission (TE) model and combining the series resistance (R_s) effect:[26,27]

$$J = A^{*}T^{2}e^{-\frac{q\varphi_b}{kT}}(e^{\frac{q(V-JAR_S)}{nkT}} - 1) \tag{1}$$

where A^* represents the Richardson constant of β-Ga_2O_3 (41 A/(cm^2·K^2)).[28] The ideality factor (n) can be deduced from the intercept of the differential equation (shown in Figure 3(b)):

$$\frac{dV}{d\ln J} = AR_sJ + \frac{nkT}{q} \tag{2}$$

yielding the values of 1.19, 1.38 and 1.07 for SBD, HJD and HJBS, respectively. Further, by defining a function $H(J)$:

$$H(J) = V - \frac{nkT}{q}\ln\frac{J}{A^{*}T^{2}} \tag{3}$$

the barrier height $q\varphi_b$ of the HJBS can be deduced to be 1.4 eV from the intercept of the equation (shown in Figure 3(c)):

$$H(J) = AR_sJ + nq\varphi_{\mathrm{b}} \tag{4}$$

Notably, the V_{on} is much smaller than the extracted barrier height $q\varphi_b$, which may be

ascribed to the defect-assisted tunneling and interface recombination at the small forward bias regime.[29]

The reverse *J-V* characteristics of the devices are illustrated in Figure 3(d). The cathode is grounded and the anode is reversely swept until the reverse leakage current dramatically increases in a sudden or reaches the breakdown criteria of 0.1 A/cm^2.[30] For the SBD, the reverse leakage current (J_R) is lower than 2 μA/cm^2 (the detection limit of the system) for the reverse bias (V_R) < 250 V. After that, J_R increases with the increase of V_R. While for the HJBS diode, J_R remains to be <2 μA/cm^2 even at a V_R of 1250 V and then increases fast to the breakdown criteria. The J_R is also comparable to that of the reported NiO/β-Ga_2O_3 HJBS diodes with similar structure,[28,31] revealing the RESURF effect arising from junction barrier Schottky structure.

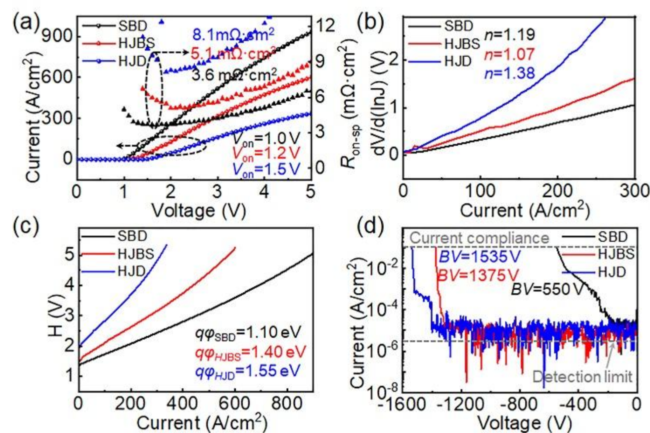

Fig. 3. (a) The forward current-voltage (*J-V)* curves and $R_{on,sp}$ of β-Ga_2O_3 SBD and SnO/β-Ga_2O_3 HJBS diode. Plots of (b) d*V*/dln*J* *versus J* and (c) H(*J*) *versus J*. (d) Reverse *J-V* characteristics of the devices.

Electric field distribution of β-Ga_2O_3 SBD and HJBS diode under 500 V reverse bias was simulated by Silvaco TCAD to reveal the mechanism for the depressed J_R and improved *BV*. As we can see from Figure 4(a) and (b), β-Ga_2O_3 SBD presents a

remarkable electric field crowding effect, giving a peak electric field of 4.5 MV/cm at the edge of the anode and leading to a premature breakdown (Figure 4(c)). For the HJBS diode, the electric field crowding effect is effectively suppressed by the JTE, presenting a relatively uniform electric field in the structure and a peak electric field decreased to 2.3 MV/cm. Meanwhile, the electric field underneath the anode of HJBS shows a fluctuation in the range of 1.36-1.18 eV corresponding to the heterojunction array structure. Clearly, due to the lateral depletion of the inner SnO/β-Ga_2O_3 p-n junction, the current channel in the Schottky region is narrowed, which can shield the Schottky contacts and reduce the reverse leakage current caused by barrier lowering effects.[28,32]

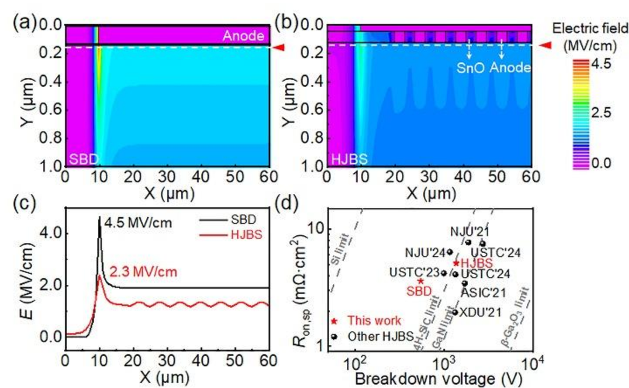

Fig. 4. Simulated electric field distribution of (a) β-Ga_2O_3 SBD and (b) β-Ga_2O_3 JBS diode under the same reverse bias (500 V). (c) Extracted electric field along the horizontal dash line (1 nm below the Schottky junction interface). (d) Benchmark plot of $R_{on,sp}$ and BV for reported state-of-art β-Ga_2O_3 diodes and this work.

The BV of the HJBS diode is measured to be 1375 V, which overpasses that of the SBD (550 V). Therefore, although the HJBS diode has a slightly increased V_{on} and $R_{on,sp}$ when compared to the SBD counterpart, it provides a much higher BV. The power figure of merit (PFOM = $BV^2/R_{on,sp}$) is calculated to be 0.37 GW/cm^2, which is comparable to that of the previously reported NiO/β-Ga_2O_3 HJBS diodes with similar structure (shown

in Table S1)[31,33] and positions the device at the forefront among β-Ga_2O_3 devices. Figure 4(d) benchmarks the $R_{on,sp}$ *vs* BV plot of the state-of-the-art β-Ga_2O_3 HJBS diodes. As marked, without adopting field limiting rings and the deep-etching process, our SnO/β-Ga_2O_3 HJBS diode presents a decent $R_{on,sp}$ and BV.

β-Ga_2O_3 HJBS diodes with various spacing (L) are also fabricated, which forward and reverse I-V characteristics are plotted in Figure 5 (a) and (b). Clearly, with the decrease of L from 5 to 3 μm, V_{on} slightly increases from 1.1 to 1.2 V. This is reasonable since a narrower spacing reduces the conduction area in unipolar mode, leading to a sacrifice in the V_{on} for a given anode area.[28] However, the BV shows a significant increase from 1155 to 1375 V, which is expected to be further improved with the shrinking spacing.

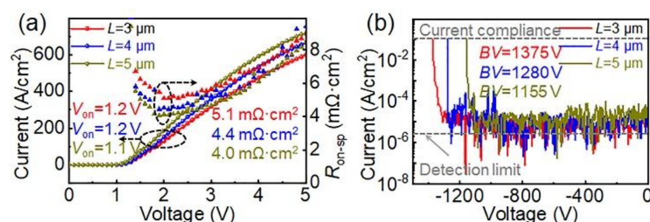

Fig. 5. (a) The forward I-V curves and $R_{on,sp}$ and (b) reverse I-V curves of the SnO/β-Ga_2O_3 HJBS diodes with spacing 3 μm, 4 μm, 5 μm, respectively.

In summary, the verticalβ-Ga_2O_3 HJBS diode is fabricated through combining with circular p-type SnO film array. Due to the depressed electric field crowding effect at the anode edge as well as the lateral depletion effect of the SnO/β-Ga_2O_3 p-n junction at high V_R, the current channel underneath the anode is narrowed, giving a suppressed J_R and an improved BV. The HJBS diode with the spacing of 3 μm shows V_{on} of 1.2 V and $R_{on,sp}$ of 5.1 mΩ·cm², which are slightly interior to the SBD but superior to the HJD, but its BV is greatly improved to 1375 V and is expected to be further improved with

the shrinking spacing. The PFOM of 0.37 GW/cm^2 positions the device at the forefront among *β*-Ga_2O_3 devices, suggesting the *β*-Ga_2O_3 HJBS diodes with *p*-type SnO film a prominent candidate for the future *β*-Ga_2O_3 power electronic devices.

Conflicts of interest

There are no conflicts to declare.

Acknowledgments

This work was supported by the National Natural Science Foundation of China (NSFC, No. 62074048), the Key Research and Development Plan of Anhui Province (No. 2022f04020007), and the Natural Science Foundation of Anhui Province (No. 2208085MF177).

Notes and references

1 A. J. Green, J. Speck, G. Xing, P. Moens, F. Allerstam, K. Gumaelius, T. Neyer, A. Arias-Purdue, V. Mehrotra, A. Kuramata, K. Sasaki, S. Watanabe, K. Koshi, J. Blevins, O. Bierwagen, S. Krishnamoorthy, K. Leedy, A. Arehart, A. Neal, S. Mou, S. Ringel, A. Kumar, A. Sharma, K. Ghosh, U. Singisetti, W. Li, K. Chabak, K. Liddy, A. Islam, S. Rajan, S. Graham, S. Choi, Z. Cheng, and M. Higashiwaki, *APL Materials*, 2022, **10**, 029201.

2 M. Higashiwaki, K. Sasaki, H. Murakami, Y. Kumagai, A. Koukitu, A. Kuramata, T. Masui, and S. Yamakoshi, *Semicond. Sci*. Technol., 2016, **31**, 034001.

3 S. J. Pearton, J. Yang, P. H. C. IV, F. Ren, J. Kim, M. J. Tadjer, and M. A. Mastro, *Appl. Phys. Reviews*, 2018, **5**, 011301.

4 K. Sasaki, M. Higashiwaki, A. Kuramata, T. Masui, and S. Yamakoshi, *IEEE Electron Device Lett.*, 2013, **34**, 493-495.

5 Y. Kokubun, S. Kubo, and S. Nakagomi, *Appl. Phys. Express,* 2016, **9**, 091101.

6 B. J. Baliga, *IEEE Electron Device Lett.*, 1984, **5**, 194-196.

7 J. Wen, W. Hao, Z. Han, F. Wu, Q. Li, J. Liu, Q. Liu, X. Zhou, G. Xu, S. Yang, and S. Long, *IEEE Trans. Electron Devices*, 2024, **71**, 1606-1617.

8 Y. Lv, Y. Wang, X. Fu, S. Dun, Z. Sun, H. Liu, X. Zhou, X. Song, K. Dang, S. Liang, J. Zhang, H. Zhou, Z. Feng, S. Cai, and Y. Hao, *IEEE Trans. Power Electron*, 2021, **36**, 6179-6182.

9 Q. Yan, H. Gong, J. Zhang, J. Ye, H. Zhou, Z. Liu, S. Xu, C. Wang, Z. Hu, Q. Feng, J. Ning, C. Zhang, P. Ma, R. Zhang, and Y. Hao, *Appl. Phys. Lett.*, 2021, **118**, 122102.

10 T. Watahiki, Y. Yuda, A. Furukawa, M. Yamamuka, Y. Takiguchi, and S. Miyajima, *Appl. Phys. Lett.*, 2017, **111**, 222104.

11 R. Zheng, W. Feng, C. Liao, H. Hu, X. Lu, J. Liang, Z. Chen, G. Wang, and Y. Pei, *IEEE Trans. Electron Devices*, 2024, **71**, 1587-1591.

12 M. Budde, D. Splith, P. Mazzolini, A. Tahraoui, J. Feldl, M. Ramsteiner, H. Von Wenckstern, M. Grundmann, and O. Bierwagen, *Appl. Phys. Lett.*, 2020, **117**, 252106.

13 J. Y. Zhang, W. W. Li, R. L. Z. Hoye, J. L. MacManus-Driscoll, M. Budde, O. Bierwagen, L. Wang, Y. Du, M. J. Wahila, L. F. J. Piper, T. -L. Lee, H. J. Edwards, V. R. Dhanak, and K. H. L. Zhang, *J. Mater. Chem. C*, 2018, **6**, 2275-2282.

14 M. Budde, P. Mazzolini, J. Feldl, C. Golz, T. Nagata, S. Ueda, G. Hoffmann, F. Hatami, W. Masselink, M. Ramsteiner, and O. Bierwagen, *Phys. Rev. Materials*, 2020, **4**, 124602.

15 J. S. Jung, S. J. Park, J. H. Ye, J. G. Woo, B. S. Bae, and E. -J. Yun, *Thin Solid Films*, 2022, **747**, 139139.

16 L. Y. Liang, Z. M. Liu, H. T. Cao, and X. Q. Pan, *ACS Appl. Mater. Interfaces*, 2010, **2**, 1060-

1065.

17 H. Luo, L. Liang, H. Cao, Z. Liu, and F. Zhuge, *ACS Appl. Mater. Interfaces*, 2012, **4**, 5673-5677.

18 K. Mashooq, J. Jo, and R. L. Peterson, *IEEE Trans. Electron Devices*, 2024, 71, 574–580.

19 H. Gong, F. Zhou, W. Xu, X. Yu, Y. Xu, Y. Yang, F. Ren, S. Gu, Y. Zheng, R. Zhang, H. Lu, and J. Ye, *IEEE Trans. Power Electron.*, 2021, 36, 12213–12217.

20 F. Zhou, H. Gong, W. Xu, X. Yu, Y. Xu, Y. Yang, F. Ren, S. Gu, Y. Zheng, R. Zhang, J. Ye, and H. Lu, *IEEE Trans. Power Electron.*, 2022, 37, 1223–1227.

21 Y. Ogo, H. Hiramatsu, K. Nomura, H. Yanagi, T. Kamiya, M. Hirano, and H. Hosono, *Appl. Phys. Lett.*, 2008, **93**, 032113.

22 Y. Zeng, H. Huang, X. Zhao, M. Ding, X. Hou, Y. Zou, J. Du, J. Liu, S. Yu, K. Han, Y. Wu, X. Zhou, G. Xu, and S. Long, *IEEE Electron Device Lett.*, 2023, **44**, 2003-2006.

23 F. Tsai, S. Wang, Y. Tu, Y. Hsu, C. Kuo, Z. Lin, and R. Ko, *Appl. Phys. Express*, 2011, **4**, 025002 .

24 X. Lu, X. Zhou, H. Jiang, K.W. Ng, Z. Chen, Y. Pei, K.M. Lau, and G. Wang, *IEEE Electron Device Lett.*, 2020, **41**, 449–452.

25 H. H. Gong, X. H. Chen, Y. Xu, F. -F. Ren, S. L. Gu, and J. D. Ye, *Appl. Phys. Lett.*, 2020, **117**, 022104.

26 S. K. Cheung, and N. W. Cheung, *Appl. Phys. Lett.*, 1986, **49**, 85-87.

27 J. G. Hao, H. H. Gong, X. H. Chen, Y. Xu, F. F, Ren, S. L. Gu, R. Zhang, Y. D. Zheng, and J. D. Ye, *Appl. Phys. Lett.*, 2021, **118**, 26160.

28 Q. Li, W. Hao, J. Liu, Z. Han, S. He, X. Zhou, G. Xu, and S. Long, *Appl. Phys. Express*, 2024, **17**, 066501.

29 H. Gong, X. Chen, Y. Xu, Y. Chen, F. Ren, B. Liu, S. Gu, R. Zhang, and J. Ye, *IEEE Trans. Electron Devices*, 2020, **67**, 3341-3347.

30 J. S. Li, C. C. Chiang, X. Xia, T. J. Yoo, F. Ren, H. Kim, and S. Pearton, *Appl. Phys. Lett.*, 2022, **121**, 042105.

31 W. Hao, Q. He, Z. Han, X. Zhao, G. Xu, S. Yang, and S. Long, *in 2023 35th International*

Symposium on Power Semiconductor Devices and ICs (ISPSD), IEEE, Hong Kong, 2023, 394-397.

32 W. Li, K. Nomoto, M. Pilla, M. Pan, X. Gao, D. Jena, and H.G. Xing, *IEEE Trans. Electron Devices*, 2017, **64**, 1635-1641.

33 H. H. Gong, X. X. Yu, Y. Xu, X. H. Chen, Y. Kuang, Y. J. Lv, Y. Yang, Y. D. Zheng, R. Zhang and J. D. Ye, *Appl. Phys. Lett.*, 2021, **118**, 202102.

Data availability statements

The data that support the findings of this study are available from the corresponding author upon reasonable request.